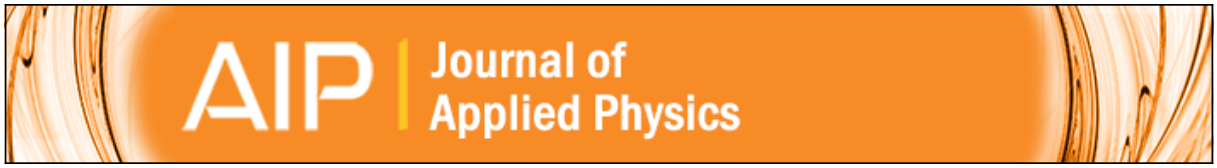

Origin of platelike granular structure for the ultrananocrystalline diamond films synthesized in H 2 -containing Ar / CH 4 plasma

Chuan-Sheng Wang, Huang-Chin Chen, Hsiu-Fung Cheng, and I-Nan Lin

Citation: Journal of Applied Physics **107**, 034304 (2010); doi: 10.1063/1.3296187

View online: http://dx.doi.org/10.1063/1.3296187

View Table of Contents: http://scitation.aip.org/content/aip/journal/jap/107/3?ver=pdfcov

Published by the AIP Publishing

Origin of platelike granular structure for the ultrananocrystalline diamond films synthesized in H_2-containing Ar/CH_4 plasma

Chuan-Sheng Wang,[1,2] Huang-Chin Chen,[1] Hsiu-Fung Cheng,[3] and I-Nan Lin[1,a)]
[1]*Department of Physics, Tamkang University, Tamsui, Taiwan 251, Republic of China*
[2]*Technology and Science Institute of Northern Taiwan, Peitou, Taipei, Taiwan 112, Republic of China*
[3]*Department of Physics, National Taiwan Normal University, Taipei, Taiwan 106, Republic of China*

(Received 5 November 2009; accepted 21 December 2009; published online 1 February 2010)

The modification on microstructure of diamond films due to the incorporation of H_2 species into the Ar/CH_4 plasma was systematically investigated. While the hydrogen-free plasma produced the ultrananocrystalline diamond films with equiaxed grains (about 5 nm in size), the hydrogen-containing plasma resulted in platelike grains (about 100×300 nm^2 in size). The size of the platelike grains increased with the H_2 content in the plasma. Transmission electron microscopy and optical emission spectroscopy reveal that only $0.1\%H_2$ incorporated in the Ar/CH_4 plasma is sufficient for inducing the formation of platelike grains, suggesting that the platelike grains are formed via the competition between the attachment and the etching of hydrocarbons onto the existing diamond surfaces. In Ar plasma, the diamond grains were always passivated with hydrocarbons and the active carbon species in the plasma can only renucleate to form nanocrystalline diamond grains. Incorporation of H_2 species in the plasma leads to partial etching of hydrocarbons adhered onto the diamond grains, such that active carbon species in the plasma can attach to diamond surface anisotropically, resulting in diamond flakes and dendrites geometry.
 [doi:10.1063/1.3296187]

I. INTRODUCTION

Diamond films possess marvelous physical and chemical properties and have great potential for device applications. Recently, main focus of research has been directed toward the synthesis and properties of ultrananocrystalline diamond (UNCD) films,[1] as the UNCD films possess many excellent properties and several of them actually exceed those of diamond.[2] When the diamond grain size in UNCD film is less than 10 nm, surface smoothness was improved markedly, making it a promising material for tribological applications.[3] The decrease in diamond grain size increases the proportion of grain boundaries, which contain nondiamond carbons. A very high electron field emission (EFE) characteristic has been reported for ultrananocrystalline films.[4,5] Moreover, unlike the syntheses of diamond films with micron-sized grains that utilized H_2 plasma and requires high substrate temperature (~900 °C), the growth of UNCD films used hydrogen free plasma,[1] which grew the UNCD films at very low substrate temperature[6,7] and is more compatible with the integrated circuits (IC) process. However, the microstructure of the UNCD films is extremely sensitive to the growth parameters, especially the constituents of the plasma.[8–11] Transition in microstructure with the plasma chemistry has been presumed due to the change in growth mechanism from CH_3 in high hydrogen plasma to C_2 in low hydrogen plasma.[11] However, the detail mechanism on how the plasma chemistry modifies the microstructure of diamond is still not completely resolved.

In the present study, we synthesized diamond films using microwave plasma enhanced chemical-vapor deposition (CVD) process with wide range of Ar/H_2 ratio and used the transmission electron microscopy (TEM) to investigate how the characteristics of plasma modified the microstructure of the diamond films. The possible mechanism for the modification of microstructure was discussed based on these observations.

II. EXPERIMENTAL

N-type mirror polished Si (100) substrates were used to grow diamond film. The substrates were first ultrasonically cleaned by acetone and then dipped in HF for 1 min to remove any surface contamination and native oxides. The substrates were ultrasonicated in a solution containing the mixture of diamond powders (30 nm) and Ti powders (325 nm) in methanol to facilitate the nucleation process. The substrates were again ultrasonically cleaned in de-ionized water to remove diamond particles sticking to the surface and then dried by blowing the nitrogen gas. The diamond films were grown by microwave plasma CVD process using an IPLAS setup (Cyrannus, 2.45GHz) for 3 h, with microwave power of 1200 W and chamber pressure of 100 torr in $(Ar_{1-x}H_x):CH_4=99:1$ SCCM (SCCM denotes cubic centimeter per minute at STP) gas mixture. The diamond films grown with small proportion of H_2 ($x=0$, 0.01, and 1.5) were designated as $UNCD_0$, $UNCD_{01}$, and $UNCD_1$, respectively, and those deposited with larger proportion of H_2 ($x=3.5\%$, 8.0%, and 20.0%) were designated as $UNCD_3$, $UNCD_8$, and $UNCD_{20}$, respectively. No external heater was used to heat the substrate and the substrate temperature was in the range of 460–475 °C due to plasma heating.

a)Author to whom correspondence should be addressed. Electronic mail: inanlin@mail.tku.tw.

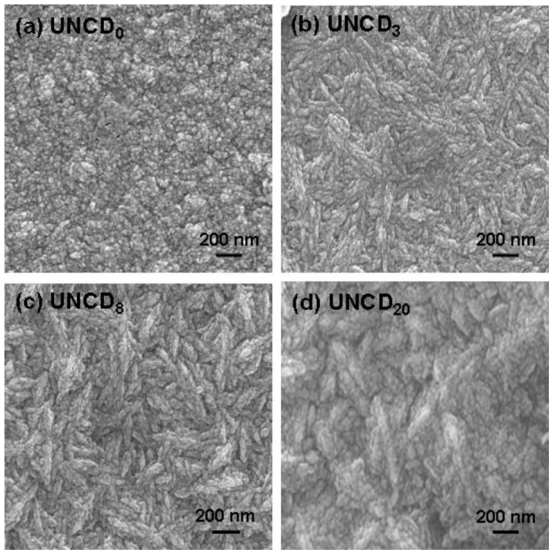

FIG. 1. The SEM micrographs for the diamond films grown in $(1-x)\mathrm{Ar}-x\mathrm{H_2}/\mathrm{CH_4}$ plasma, where x=(a) 0% ($\mathrm{UNCD_0}$), (b) 3.5% ($\mathrm{UNCD_3}$), (c) 8.0% ($\mathrm{UNCD_8}$), and (d) 20.0% ($\mathrm{UNCD_{20}}$).

The surface morphologies and the microstructure of the diamond films were examined by FE-SEM (JEOL JSM-6500F) and TEM (Joel 2100), respectively. The crystalline quality of the deposited diamond films was characterized by Raman spectroscopy (Renishaw) using 514 or 325 nm laser beams. The EFE properties of the diamond films were measured using a parallel-plate setup, under 10^{-6} torr. The gap between the anode tip (1 mm diameter) and the cathode was adjusted by a micrometer. The current-voltage characteristics of the films were acquired using a Keithley 2410 electron source unit and were modeled by Fowler–Nordheim (FN) theory.[12] The turn-on field was designated as the interception of the straight lines extrapolated from the low field and high field segments of the FN plots, viz., $\log(\mathrm{J}/E^2)$-$1/E$.

III. RESULTS AND DISCUSSION

Effect of large proportion of $\mathrm{H_2}$ added in the $\mathrm{Ar}/\mathrm{CH_4}$ plasma on the characteristics of the diamond films was investigated first. SEM micrographs in Fig. 1 indicate that incorporation of $\mathrm{H_2}$ species into the $\mathrm{Ar}/\mathrm{CH_4}$ plasma modified the morphology of the diamond films profoundly. Contrary to the equiaxed geometry for $\mathrm{UNCD_0}$ films grown in hydrogen-free plasma [$\mathrm{UNCD_0}$, Fig. 1(a)], the grains for the films grown in $\mathrm{H_2}$-containing plasma are elongated, about 20×200 $\mathrm{nm^2}$ in size [$\mathrm{UNCD_3}$, Fig. 1(b)]. The size of elongated grains increases with the $\mathrm{H_2}$ content in the plasma [$\mathrm{UNCD_8}$, Fig. 1(c)]. Finally, the grains agglomerate to form clusters about a few hundreds of nanometers for the films grown in 20%$\mathrm{H_2}$ plasma [$\mathrm{UNCD_{20}}$, Fig. 1(d)].

Visible Raman spectroscopy (514 nm) for $\mathrm{UNCD_0}$ samples [spectrum I, Fig. 2(a)] indicates that they contain very broad Raman peaks, typical characteristics of ultrasmall grain diamond materials.[13] Deconvolution of this spectrum indicates the presence of the D^* band (1350 $\mathrm{cm^{-1}}$) and G band (1580 $\mathrm{cm^{-1}}$), representing disordered carbons and graphite,[14] respectively, and the ν_1 band (1140 $\mathrm{cm^{-1}}$) and ν_2 bands (1480 $\mathrm{cm^{-1}}$), representing *trans*-polyacetylene[15] existing in grain boundaries. No sharp D-band Raman peak at 1332 $\mathrm{cm^{-1}}$, the characteristics of sp^3-bonded diamonds, was observable. The intensity of the sp^2-related bands (except the G band) increases with the $\mathrm{H_2}$ content in the plasma [spectrums II to IV, Fig. 2(a)]. While the visible Raman is sensitive to the sp^2 bonds and is good for detecting the presence of the disorder carbons in the samples, it is not suitable for examining the characterization of sp^3 bonds in UNCD films. UV Raman spectroscopy is needed for this purpose. Typical UV Raman spectroscopy (325 nm) for these films is shown in Fig. 2(b). This figure indicates that the sp^2-bonding related peaks (D^*, G, ν_1, and ν_2 bands) are pronouncedly smaller in UV Raman spectra, as compared with those in visible Raman spectra.[16] The D band at 1332 $\mathrm{cm^{-1}}$ is clearly observable for all UNCD samples and the relative proportion of sp^3 band increases monotonously with the $\mathrm{H_2}$ content in the Ar plasma. Although the UV Raman is relatively insensitive to the sp^2 bonds and is more suitable for examining the characteristics of the sp^3 bonds in the films, these Raman spectroscopies are still not able to unambiguously identify that the materials are diamond. TEM microscopic examinations on these samples are necessary.

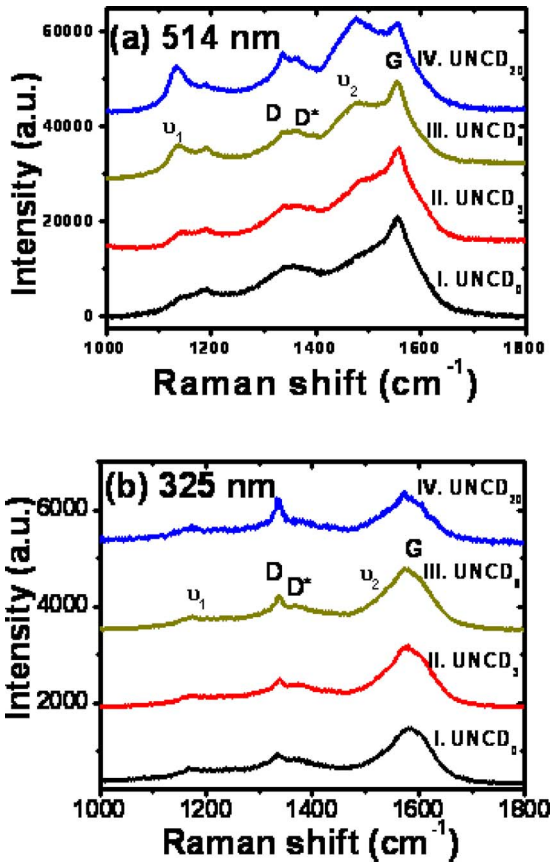

FIG. 2. (Color online) The (a) visible and (b) UV Raman spectroscopies for the diamond films grown in $(1-x)\mathrm{Ar}-x\mathrm{H_2}/\mathrm{CH_4}$ plasma, where x=0% ($\mathrm{UNCD_0}$), 3.5% ($\mathrm{UNCD_3}$), 8.0% ($\mathrm{UNCD_8}$), and 20.0% ($\mathrm{UNCD_{20}}$).

TEM micrographs in Fig. 3 reveal that, while the grains for $\mathrm{UNCD_0}$ films are of spherical geometry with ultrasmall size [Fig. 3(a)], the elongated grains for $\mathrm{UNCD_3}$ films grown in 3%$\mathrm{H_2}/\mathrm{Ar}$ plasma are of rod-shaped geometry [Fig. 3(b)]. For the $\mathrm{UNCD_8}$ films grown in 8%$\mathrm{H_2}/\mathrm{Ar}$ plasma, the grains

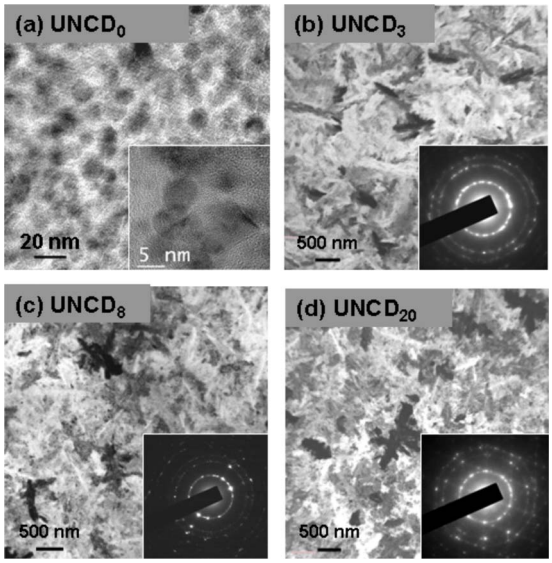

FIG. 3. (Color online) The TEM micrographs for the diamond films grown in $(1-x)\mathrm{Ar}-x\mathrm{H_2}/\mathrm{CH_4}$ plasma, where x=(a) 0% ($\mathrm{UNCD_0}$), (b) 3.5% ($\mathrm{UNCD_3}$), (c) 8.0% ($\mathrm{UNCD_8}$), and (d) 20.0% ($\mathrm{UNCD_{20}}$).

are also of rod shaped of the same size [Fig. 3(c)], but the proportion of the elongated grains is larger and the grains intrude one another, forming dendrite geometry. The size of the dendrites increases with the H_2 content in the plasma [$\mathrm{UNCD_{20}}$, Fig. 3(d)]. Structure image shown as inset in Fig. 3(a) and the selected area electron diffractions (SAEDs) shown as insets in Figs. 3(b)–3(d) illustrate clearly that both the equiaxed and the elongated grains are diamonds, which will be more detailed investigated shortly.

Transition in microstructure with the composition of the plasma observed above is in accord with the previous observations.[11] It has been explained by the assumption that the change in granular structure is due to the change in growth process from CH_3 in high hydrogen plasma to C_2 in low hydrogen plasma.[11] However, the detail mechanism on how the plasma chemistry modifies the microstructure of diamond is still not completely resolved. There still remained questions concerning: (i) how the presence of H_2 in the Ar plasma induces the change in geometry of the diamond grains and (ii) how much H_2 is needed in order to initiate such a change. To understand these phenomena, the characteristics of UNCD films grown in smaller proportion of H_2 (0.1% and 1.5%) were investigated, and the corresponding samples were designated as $\mathrm{UNCD_{01}}$ and $\mathrm{UNCD_1}$ films, respectively. TEM micrographs shown in Figs. 4(a) and 4(b) reveal that the granular structure of the UNCD films grown in a plasma containing smaller proportion of hydrogen is also markedly different from the equiaxed geometry of the ultrasmall size grains in $\mathrm{UNCD_0}$. Large spherical clusters, around 30 nm in size, were observed for $\mathrm{UNCD_{01}}$ films and elongated clusters, around 30×200 nm in size, were observed for $\mathrm{UNCD_1}$ ones, coexisting with the matrix of ultrasmall spherical grains. These large clusters, spherical or elongated, are uniformly distributed over the samples. The corresponding SAEDs [insets, Figs. 4(a) and 4(b)] indicate that both the large clusters and the ultrasmall grains in the matrix are diamonds.

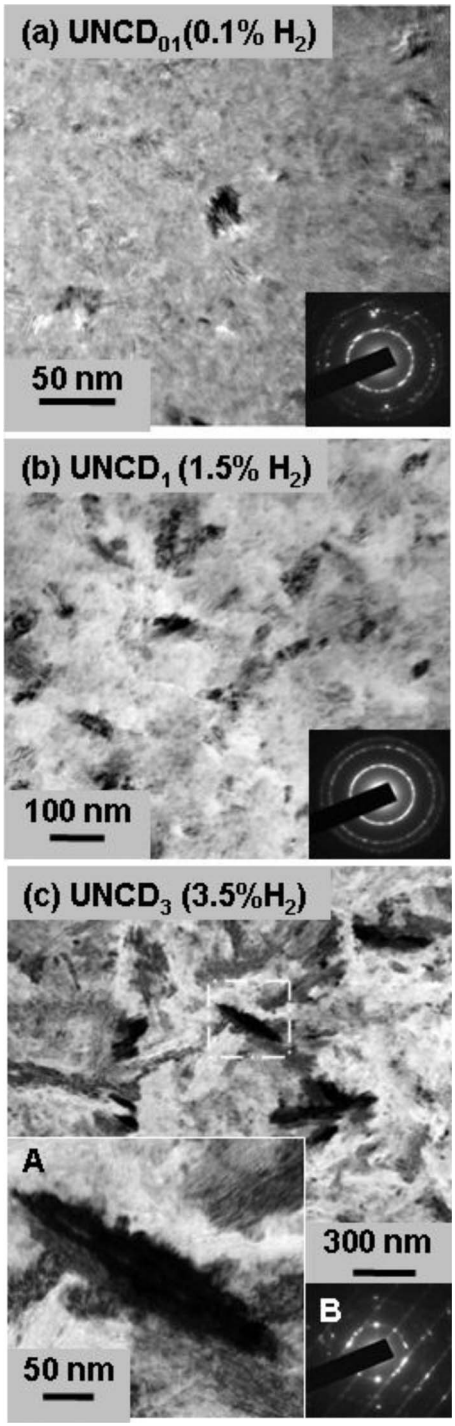

FIG. 4. The TEM micrographs for the UNCD films grown in $(1-x)\mathrm{Ar}-x\mathrm{H_2}/\mathrm{CH_4}$ plasma, where x=(a) 0.1%, $\mathrm{UNCD_{01}}$, (b) 1.5%, $\mathrm{UNCD_1}$, and (c) 3.5%, $\mathrm{UNCD_3}$.

Figure 5(a) shows that the incorporation of small amount of H_2 into Ar plasma insignificantly alters their UV Raman spectroscopies, where the Raman spectrum for $\mathrm{UNCD_0}$ samples was included to facilitate the comparison. The Raman resonance peaks are all very broad due to the smallness of the diamond grains. All the Raman spectra contain υ_1 band (1140 $\mathrm{cm^{-1}}$) and υ_2 bands (1480 $\mathrm{cm^{-1}}$), the *trans*-polyacetelyne phase,[13,14] and D^* band (1350 $\mathrm{cm^{-1}}$) and G band (1580 $\mathrm{cm^{-1}}$), the disrodered carbons, and graphitic phases.[15,16] The EFE properties of the films were only mod-

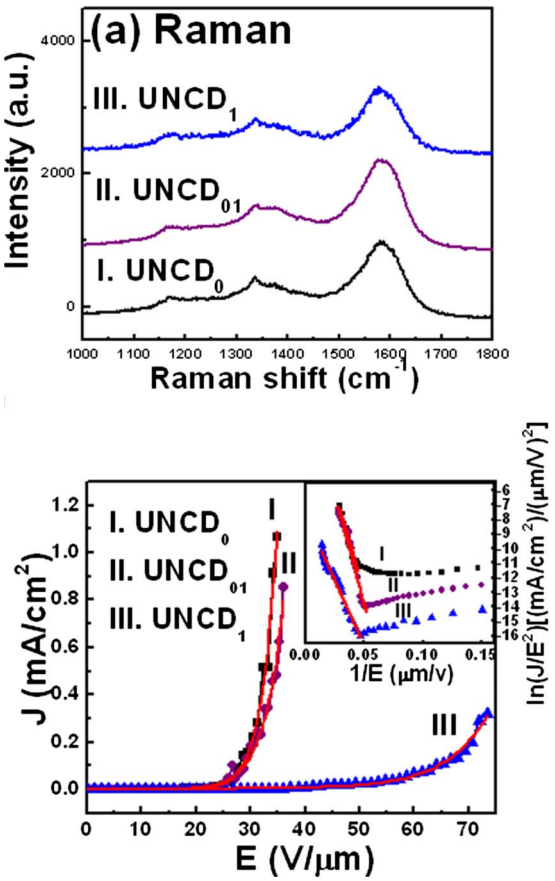

FIG. 5. (Color online) The (a) UV Raman spectroscopies and (b) EFE properties along with the FN plots for the diamond films grown in $(1-x)\mathrm{Ar}-x\mathrm{H_2}/\mathrm{CH_4}$ plasma, where x= (a) 0%, $\mathrm{UNCD_0}$, (b) 0.1%, $\mathrm{UNCD_{01}}$, and (c) 1.5%, $\mathrm{UNCD_1}$.

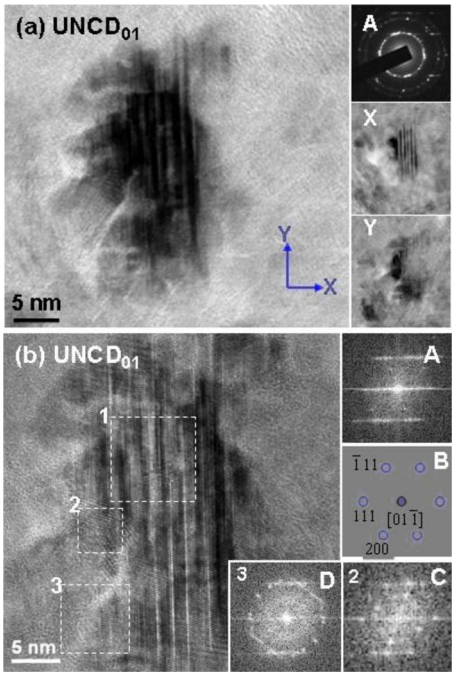

FIG. 6. (Color online) The (a) enlarged TEM micrographs of a typical region for the diamond films grown in $\mathrm{Ar}-0.1\%\mathrm{H_2}/\mathrm{CH_4}$ plasma with inset A showing SAED of this region and the insets X and Y show the image of the same area tilted for a few degree around the x and y axes, respectively; (b) the structural image of the same region in (a) with inset A showing FT images of region "1" and inset B showing the schematics of the SAED. The insets C and D show the FT images of regions "2" and "3."

erately modified due to the addition of $0.1\%\mathrm{H_2}$ in the plasma [curves I and II, Fig. 5(b)]. The turn-on field was increased from $(E_0)_{\mathrm{UNCD_0}}=20.1\ \mathrm{V}/\mu\mathrm{m}$ for $\mathrm{UNCD_0}$ films to $(E_0)_{\mathrm{UNCD_{01}}}=21.3\ \mathrm{V}/\mu\mathrm{m}$ for $\mathrm{UNCD_{01}}$ films. The EFE current densities for these films are about the same, i.e., $(J_e)_{\mathrm{UNCD_0}}=0.8-1.0\ \mathrm{mA/cm^2}$ at 35 $\mathrm{V}/\mu\mathrm{m}$ applied field. In contrast, the EFE properties were markedly altered when only slightly larger amount of hydrogen $(1.5\%\mathrm{H_2})$ was incorporated into in Ar plasma. Curve III in Fig. 5(b) shows that the turn-on field was increased to $(E_0)_{\mathrm{UNCD_1}}=23.2\ \mathrm{V}/\mu\mathrm{m}$ with the EFE current density markedly lowered to $(J_e)_{\mathrm{UNCD_1}}=0.3\ \mathrm{mA/cm^2}$ at 75 $\mathrm{V}/\mu\mathrm{m}$ applied field for $\mathrm{UNCD_1}$ films, which were essentially nonemitting at 35 $\mathrm{V}/\mu\mathrm{m}$ applied field. The EFE characteristics of the UNCD films were degraded even more when larger proportion of $\mathrm{H_2}$ was incorporated in the plasma (figures not shown). The TEM microscopy and the EFE measurements imply clearly that the transition in microstructure has already been initiated when only $0.1\%\mathrm{H_2}$ was incorporated into Ar plasma.

To understand the mechanism that alter the EFE characteristics for the UNCD films, the detailed microstructure of these UNCD films were examined using TEM. Figure 6(a) illustrates the bright field image for one of the typical diamond cluster in the $\mathrm{UNCD_{01}}$ films, which were grown in $\mathrm{Ar}-0.1\%\mathrm{H_2}$ plasma, revealing that the clusters ($\sim$10 $\times$20 nm) contain parallel fringes. The ring shaped SAED patterns [inset A, Fig. 6(a)] indicate that the matrix embedding the large clusters contains randomly oriented diamond grains, whereas the streaks associated with the major diffraction spots imply that the fringes in the large clusters are platelike defects. The insets X and Y of this figure reveal that the appearance of the images changes when the samples were tilted a few degrees around the x and y axes, respectively. Notably, the x axis and y axis are, respectively, in parallel with and perpendicular to the [111] axis of the UNCD crystals, which will become evident when we examine these images in detail. Inset X shows that the fringes in platelike defects are always visible when the samples were tilted around [111] direction, the x axis, that keep the (111) plane in parallel with the electron beams. But these fringes disappear when the sample was titled around y axis (inset Y) that tilted the (111) planes away from the electron beams. These results confirm again that the fringes are platelike defects lying on (111) lattice plans. Such an argument will be further supported by the structure images of the same region that will be discussed below.

Figure 6(b) illustrates the structure image of the same region shown in Fig. 6(a), indicating that the platelike defects contain large proportion of stacking faults. Fourier-transformed (FT) images of region "1" shown as inset A in this figure and the schematics of this diffraction pattern shown as inset B indicate that the samples are near $[01\bar{1}]$ zone axis and the streaks are along [111] direction. That is, the platelike defects are stacking faults (or twins) lying on (111) lattice planes. Insets C and D in Fig. 6(b) shows the FT

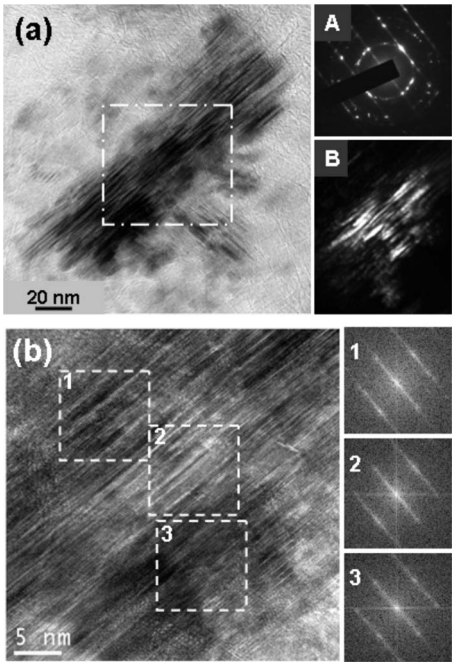

FIG. 7. The (a) enlarged TEM micrographs of a typical region for the $UNCD_1$ diamond films that were grown in $Ar-1.5\%H_2/CH_4$ plasma with inset A showing SAED of this region and the inset B showing the dark field image of the same area; (b) the structure image of the central region in "a" with the insets showing the FT images of the designated areas.

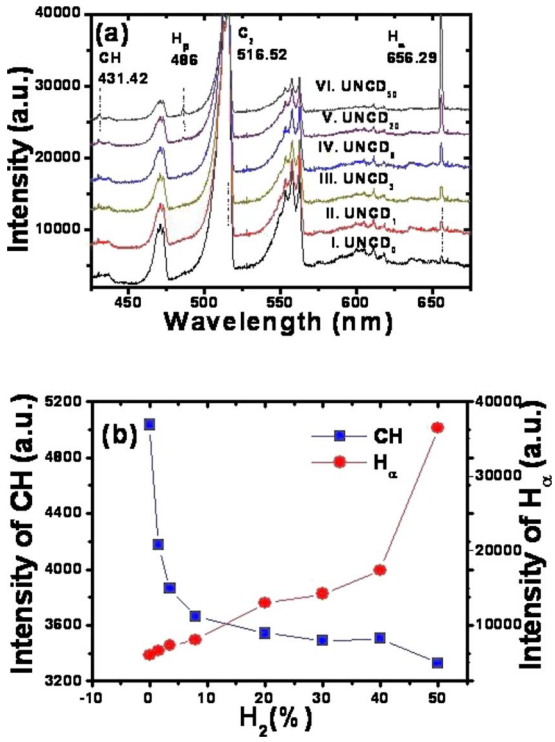

FIG. 8. (Color online) (a) The optical emission spectroscopy of the $(1-x)Ar-xH_2/CH_4$ plasma used for growing the diamond films, where $x=0\%(UNCD_0)$, $1.5\%(UNCD_1)$, $3.5\%(UNCD_3)$ $8\%(UNCD_8$, $20\%(UNCD_{20}$, and $50\%(UNCD_5)$; (b) the variation in CH and H_α line intensity with the H_2 content in the plasma.

images (FT_2 and FT_3) corresponding to regions 2 and 3, respectively, revealing that these regions are also diamonds with $[01\bar{1}]$ zone axis. However, extra spots corresponding to *i carbon*, an allotropic phase of cubic diamond, appear in FT_2 and diffuse rings corresponding to amorphous carbon or (graphite) appear in FT_3. These observations imply that the phase transformation process has occurred. Presumably, the platelike clusters are formed by Ostward ripening process, in which the spherical grains grew anistropically along (111) lattice plane, annihilating the adjacent grains. The outward diffusion of carbons from adjacent region toward platelike clusters may transform the diamond in this region into *i* carbon or graphite.

Moreover, the microstructure of the $UNCD_1$ samples that were grown in $1.5\%H_2$-Ar plasma was shown in Fig. 7(a). This figure reveals that the clusters in $UNCD_1$ samples also contain fringes, but are larger ($\sim 40\times 160$ nm in size). The SAED pattern of these clusters [inset A, Fig. 7(a)] contains streaks oriented along the [111] direction, implying again that the fringes in TEM micrograph are, again, the edge-on (111) planes, i.e., the clusters are platelike grains. Dark field image [inset B, Fig. 7(a)] further confirms that the streaks in the SAED pattern are contributed from the platelike grains. The platelike grains are distributed uniformly over the samples and are the typical granular structure of the $UNCD_1$ samples. Figure 7(b) shows the structure image of the central region of the platelike grains [indicated in Fig. 7(a)]. The FT images of the designated areas [insets 1, 2, and 3, Fig. 7(b)] reveal that these areas belong to the same diamond grains. The streaks in the FT images indicate, again, that the straight fringes are actually the edge-on (111) lattice planes. Moreover, Fig. 4(c) illustrates the enlarged TEM image of $UNCD_3$ films, which were grown in $3.5\%H_2$ plasma. It is clearly observed that the films contain aggregates of platelike grains orientated in different directions. Each of the platelike grains is of similar microstructure with those shown in Fig. 7 (figure not shown). In other words, in $UNCD_3$-$UNCD_{20}$ samples the number density and the size of the platelike grains increase with the H_2 content in the plasma, such that the platelike grains intrude one another, forming dendrite geometry.

The optical emission spectroscopy (OES) of the plasma was examined to investigate how the addition of H_2 into the plasma modifies the microstructure of the UNCD films. Figure 8(a) shows the typical OES spectra of the plasma used for growing these UNCD films. To facilitate the comparison, the OES of a plasma containing $50\%H_2$ was also included in Fig. 8(a) as OES-VI. The Ar/CH_4 plasma [OES-I, Fig. 8(a)] is predominated with the Swan band near 474.7, 516.5, and 563.5 nm,[17] which are mainly the emissions from the C_2 species. There also exist a spectral line from CH species (431 nm) and a small spectral line corresponding to atomic hydrogen species, H_α (656.3 nm).[18,19] The intensity of H_α line increases and those of CH lines and Swan band decreases, as the proportion of H_2 added in the plasma increases [Fig. 8(b)]. There appears a small H_β (486 nm) line in OES-V (and OES-VI) that corresponds to the 20% (and $50\%)H_2-Ar$ plasma.

It is known that the electron temperature (T_e) of the plasma can be estimated using the Boltzmann plots,[20,21] viz.,

$$\frac{I_{ji}}{I_{kj}} = \frac{\lambda_{kl} A_{ji} g_j}{\lambda_{ji} A_{kj} g_k} \exp\left(\frac{E_k - E_j}{k_B T_{ex}}\right), \quad (1)$$

where I_{ji} and λ_{ji} are the intensity and wavelength of the spectral line corresponding to the transition between E_j and E_i energy level; k_B is the Boltzmann constant; A_{ji} and g_j is, respectively, the corresponding Einstein transition probability and statistical weight, which can be acquired from the literature.[22] Only the OES-V (and OES-VI) shows clear H_β and H_α lines that can be used for estimating the electron temperature, resulting in $(T_e)_{UNCD_{20}} = 10\,252$ K and $(T_e)_{UNCD_{50}} = 13\,550$ K. The intensity of H_β line for $UNCD_1$-$UNCD_8$ samples is too weak to evaluate the electron temperature of the corresponding plasma. However, these OES spectra imply that, although the presence of H_β line cannot be clearly resolved for $UNCD_1$-$UNCD_8$ plasma, the proportion of atomic hydrogen species and the plasma temperature generated in the plasma are expected to increase with the H_2 species incorporated into the Ar/CH_4 plasma. How the presence of active hydrogen modifies the granular structure for diamond films will be discussed in the following section.

IV. DISCUSSION

The formation mechanism for UNCD films grown in Ar-rich plasma was originally suggested[23] that the C_2 radical played an important role in the growth mechanism, but recent investigations[24–26] argued that it is the competition between H atoms, CH_3 radicals, and other C_1 species, reacting with dangling bonds on the surface that determine the renucleation behavior and hence the morphology of the diamond film. Although the mechanisms for the formation of UNCD films are still controversial, what is clear is that the carbon species induced in Ar-plasma are extremely active and renucleate easily. Presumably, the CH species present in the Ar/CH_4 plasma can adhere to the newly formed nanodiamond clusters instantaneously, forming hydrocarbon layer (transpolyacetylene).[5] The *trans*-polyacetylene layer surrounding the nanosized diamond clusters hindered the direct contact of the active carbon species in the plasma with the diamond surface. Therefore, the incoming active carbon species in the plasma can only renucleate to form another nanosized diamond clusters, rather than attach to the existing diamond surface to enlarge the size of the diamond clusters. In other words, simultaneous appearance of the CH species and the active carbon species in the plasma facilitates the formation of nanodiamond grains. Therefore, the granular structure of the UNCD films does not change with the film thickness (the growth time). Such a model is schematically illustrated in Fig. 9(a).

When large concentration of H_2 (e.g., >50%) was incorporated into the plasma, the proportion of atomic hydrogen is large and the activity of hydrogen species is high. The atomic hydrogen can efficiently etch the hydrocarbons (transploy-acetylene) adhered on the surfaces of diamonds and the active carbon species in the plasma can attach to the surface of diamonds to form sp^3 bonds, enlarging the diamond grains isotropically and resulting in large-grain granular structure

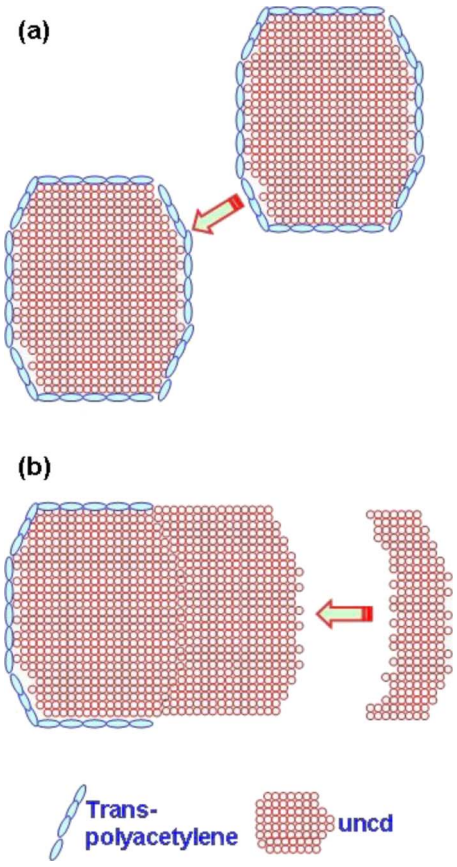

FIG. 9. (Color online) The schematic drawings for the (a) formation of UNCD ultrananograins grown in Ar plasma, in which, the nanoclusters will be instantaneously passivated by the transpolyacetylene; and (b) anisotropic growth of diamond grains grown in hydrogen-containing Ar plasma due to preferential etching of the adhered transpolyacetylene.

for the diamond films. In this case, the only factor, which influences the geometry of the diamond grains, is the competition between the intrinsic surface energy (γ) for each lattice planes. The surface with low γ will grow preferentially, resulting in the unique faceted granular structure for the diamonds. The grain size for these films increases with the growth time, resulting in columnar structure.

On the other hand, when only small proportion of H_2 was incorporated into the plasma, the induced atomic hydrogen is of too small concentration and is not active enough to etch the diamond surfaces isotropically. Only the hydrocarbons attaching to the high-γ sites were preferentially etched away and can the active carbon species in the plasma adhere to these surfaces, leading to the anisotropic growth of the diamond clusters and forming diamond flakes. Such a model is schematically illustrated in Fig. 9(b). The diamond flakes increase in proportion with the H_2 content in the plasma and finally agglomerate to form dendrite geometry. Such a process can account for the unique microstructure for the other UNCD samples grown under $3\%-20\%H_2/Ar$ plasma.

Restated, the nanoclusters formed by active carbon species in the plasma will be instantaneously passivated by the transpolyacetylene. Only when the presence of active atomic hydrogen is of high enough concentration that can efficiently etch away the adhered hydrocarbons, exposing the diamond surface, can the active carbon species in the plasma attach to

the diamond cluster, enlarging the clusters. Otherwise, the active carbon species in the plasma will renucleate by themselves to form nanodiamond clusters, resulting in UNCD films. The superior EFE properties for the $UNCD_0$ samples, as compared with those for other films, can be attributed to the existence of larger proportion of grain boundaries that contain transpolyacetylene, providing a good electron conduction path that facilitates the EFE process.[1] Incorporation of H_2 species in the plasma induces the anisotropic growth of the diamond grains and reduces the proportion of grain boundaries in the diamonds, thus increasing the turn-on field and decreasing the current density for the diamond films.

V. CONCLUSION

Incorporation of H_2 species into Ar plasma was observed to markedly alter the microstructure of diamond films. While the Ar/CH_4 plasma resulted in UNCD films with equiaxed grains ($\sim$5 nm), the H_2-containing Ar plasma lead to platelike diamond grains. The size of grains increases with H_2 content in the plasma. Optical emission spectroscopies indicated that addition of H_2 species in the Ar/CH_4 plasma lead to the decrease in CH species and increase in atomic hydrogen species. The H_2 containing plasma can partially etch away the hydrocarbons (transpolyacetylene) adhered onto the diamond clusters such that the active carbon species in the plasma can attach to diamond surface anisotropically, forming platelike diamond grains. The amount of platelike grains increased with the H_2 content in the plasma and evolved into dendrite geometry. The proportion of grain boundaries decreased that raised the turn-on field necessary for inducing the EFE process and lowered the EFE current density.

ACKNOWLEDGMENTS

The authors would like to thank the National Science Council, Republic of China for the support of this research through the Project No. NSC 96-2112-M032-011-MY3.

[1] D. M. Gruen, Annu. Rev. Mater. Sci. **29**, 211 (1999).
[2] J.A. Carlisle and O. Auciello, Electrochem. Soc. Interface **12**, 28 (2003).
[3] V. Mortet, O. Elmazria, M. Nesladek, M. B. Assouar, G. Vanhoyland, J. D'Haen, M. D. Olieslaeger, and P. Alnot, Appl. Phys. Lett. **81**, 1720 (2002).
[4] W. Zhu, G. P. Kochanski, and S. Jin, Science **282**, 1471 (1998).
[5] K. Wu, E. G. Wang, Z. X. Cao, Z. L. Wang, and X. Jiang, J. Appl. Phys. **88**, 2967 (2000).
[6] X. Xiao, J. Birrell, J. E. Gerbi, O. Auciello, and J. A. Carlisle, J. Appl. Phys. **96**, 2232 (2004).
[7] D. Pradhan, Y. C. Lee, C. W. Pao, W. F. Pong, and I. N. Lin, Diamond Relat. Mater. **15**, 2001 (2006).
[8] A. Jiao, A. Sumant, M. A. Kirk, D. M. Gruen, A. R. Krauss, and O. Auciello, J. Appl. Phys. **90**, 118 (2001).
[9] T. S. Yang, J. Y. Lai, C. L. Chen, and M. S. Wong, Diamond Relat. Mater. **10**, 2161 (2001).
[10] J. Birrell, J. E. Gerbi, O. Auciello, J. M. Bibson, J. Jonson, and J. A. Carlisle, Diamond Relat. Mater. **14**, 86 (2005).
[11] D. Zhou, D. M. Gruen, L. C. Qin, T. G. McCauley, and A. R. Krauss, J. Appl. Phys. **84**, 1981 (1998).
[12] R. H. Fowler and L. W. Nordhlim, Proc. R. Soc. London, Ser. A **119**, 173 (1928).
[13] Z. Sun, J. R. Shi, B. K. Tay, and S. P. Lau, Diamond Relat. Mater. **9**, 1979 (2000).
[14] J. Michler, Y. Von Kaenel, J. Stiegler, and E. Blank, J. Appl. Phys. **83**, 187 (1998).
[15] A. C. Ferrari and J. Robertson, Phys. Rev. B **63**, 121405 (2001).
[16] A. C. Ferrari and J. Robertson, Phys. Rev. B **61**, 14095 (2000).
[17] H. Zhou, J. Watanable, M. Miyake, A. Ogino, M. Nagatsu, and R. Nhou, Diamond Relat. Mater. **16**, 675 (2007).
[18] J. Ma, N. Michael, R. Ashfold, and Y. A. Mankelevich, J. Appl. Phys. **105**, 043302 (2009).
[19] G. Balestrino, M. Marinelli, E. Milani, A. Paoletti, I. Pinter, A. Tebano, and P. Paroli, Appl. Phys. Lett. **62**, 879 (1993).
[20] M. L. Brake and T. E. Repetto, IEEE Trans. Plasma Sci. **17**, 60 (1989).
[21] Y. Kaga, S. Tsuge, K. Kitagawa, and N. Arai, Microchem. J. **63**, 34 (1999).
[22] NIST ATOMIC SPECTRA DATABASE (version 3.1.2) (http://physics.nist.gov/asd3).
[23] D. Zhou, T. G. McCauley, L. C. Qin, A. R. Krauss, and D. M. Gruen, J. Appl. Phys. **83**, 540 (1998).
[24] P. W. May, Yu. A. Mankelevich, J. N. Harvey, and J. A. Smith, J. Appl. Phys. **99**, 104907 (2006).
[25] J. R. Rabeau, P. John, J. I. B. Wilson, and Y. Fan, J. Appl. Phys. **96**, 6724 (2004).
[26] P. W. May and Yu. A. Mankelevich, J. Phys. Chem. C **112**, 12432 (2008).